Measuring Plasma Modes near the Cyclotron Frequency in a Finite Non-Neutral Plasma: A Search for Bernstein Modes

William Hall

A senior thesis submitted to the faculty of
Brigham Young University
in partial fulfillment of the requirements for the degree of

Bachelor of Science

Bryan Peterson, Advisor

Department of Physics and Astronomy

Brigham Young University

April 2012

ABSTRACT

Measuring Plasma Modes near the Cyclotron Frequency in a Finite
Non-Neutral Plasma: A Search for
Bernstein Modes

William Hall
Department of Physics and Astronomy
Bachelor of Science

Bernstein modes are modes that propagate perpendicular to the magnetic field near the ion cyclotron frequency. The BYU Ion Experiment is in a unique position to measure the $m = 0$ azimuthally symmetric Bernstein mode in a pure ion non-neutral plasma, which has yet to be measured experimentally. Work on the experiment has developed some of the tools necessary for this measurement. However the experiment is still not able to reach a fraction of the Brillouin density limit necessary to measure the modes, and other problems with timing and density consistency remain barriers to this measurement. Steps to rectify these problems are underway, most notably implementing a pulse forming network to lengthen arc times at the source, thereby increasing plasma densities.

Keywords: plasma, Bernstein Modes, cyclotron resonance, ^{7}Be

ACKNOWLEDGMENTS

I'd like to acknowledge, first and foremost, Dr. Bryan Peterson for his patience, help, and perseverance working with me on this project. I began knowing little, and now know a little more than little, but any knowledge I've gained has largely come through his tutelage. I'd also like to acknowledge Dr. Grant Hart, Dr. Ross Spencer, and the members of the BYU Plasma Group for their patience with my eccentricities. Finally, let me acknowledge Dr. Dan Dubin of the University of California at San Diego for his stimulating discussion on the Brillouin Density Limit.

Contents

Chapter 1

Introduction

1.1 Plasma

The majority of non dark-matter mass in the universe consists of matter of the fourth state, plasma, and study of the properties and functions of these plasmas constitute heavy areas of modern research. In astrophysics, plasmas are an almost ubiquitous substance, and nearly every discipline studies them. Researchers of solar physics study plasmas in an effort, among other things, to elucidate movement and properties of solar flares, electron beams, and propagating solar radiation [1]. Interplanetary and interstellar matter is largely plasma, and use of magnetohydrodynamics (MHD) to explain their behavior constitutes a large part of theoretical research into these plasmas. Many other astrophysical phenomena use MHD and other aspects of plasma physics to explain their behavior.

Plasma phenomena are not limited to the celestial sphere. On earth, where most of the matter human beings interact with isn't ionized, plasmas still abound. A flash of lightning consists of an atmospheric electron plasma. Neon signs, plasma televisions, arc welders, and a variety of other industrial products utilize plasmas in various forms. Properties of plasmas and their uses

are now being further studied for their possible applications in magnetic confinement fusion and the International Tokamak Experimental Reactor (I.T.E.R.) is a prime example of studies in this area [2].

It perhaps goes without saying that fusion energy has been the driving force behind plasma research for the last 50 years, and with good reason. Fusion appears to offer a nearly limitless supply of fuel (the majority of the matter consists of hydrogen, the primary fuel for a fission reactor), and fusion reactors appear theoretically safer than any currently used power source in the world. Unfortunately, fusion research hasn't progressed as quickly as was once thought, largely due to difficulties in confining and maintaining the plasmas required to reach the break-even level in fusion plasmas. Current research in plasmas therefore largely focuses on solving problems related to confining, heating, and maintaining a sustainable fusion power source, and constitutes a challenging area of research with possibly great rewards.

1.2 Non-Neutral Plasmas

Most of the plasmas mentioned earlier are neutral plasmas, or in other words, plasmas consisting of a quasi-neutral mixture of both positively and negatively charged particles, typically a species of ion and electrons, as is in the typical fusion reactor. The plasma may have locally visible charge imbalances, but over the volume of the plasmas, the negative and positive charges should equal each-other, making the plasma charge-neutral on the whole.

A smaller, yet significant area of plasma research lies in the study of non-neutral plasmas. Non-neutral plasmas attempt, through various methods, either to remove one type of charge or to load in only charges of a single species, hence the plasma isn't charge neutral. These types of plasmas are vital in many areas of past and current research, and have found niches in many areas. Those areas include experiments with positron plasmas at the University of California, San Diego [3],

experiments with anti-protons and anti-hydrogen at CERN [4,5], Fourier Transform Ion Cyclotron Resonance Mass spectrometry (FTICR-MS) [6], and other broad areas of application [7]. The BYU Ion Experiment uses methods similar to these when capturing plasmas.

Non-neutral plasmas represent a unique way to study plasmas. Unlike neutral plasmas, non-neutral plasmas consist of a single species, and as such have a number of experimental advantages over their neutral counterparts. Due to conservation of canonical angular momentum, a non-neutral will diffuse more slowly than a neutral plasma, allowing for theoretically infinite confinement times [8]. Further, non-neutral plasmas, in addition to utilizing diagnostic techniques used with neutral plasmas, can use diagnostics unfit in for use with neutral plasmas, such as FTICR-MS [6].

1.2.1 Malmberg-Penning trap

Plasmas are often confined in the Penning trap, but for non-neutral plasmas, a more common variant of the Penning trap is the Malmberg-Penning trap. In the Malmberg-Penning trap, a long cylindrical metal tube is surrounded by a solenoid with many turns. The solenoid provides a magnetic field which confines the ions radially into the trap. The metal tube is separated into sections which can be individually brought to different potentials, which in turn serve as soft walls, confining the plasma. A simple schematic of a Malmberg-Penning trap is depicted in figure 1.1. The specific setup of the BYU Ion Experiment, including its trap, will be discussed in chapter 2.

1.2.2 Sources

Plasma sources range from simple electron filaments such as those used in Malmberg's original traps in the late 70's, to far more exotic sources. The ALPHA anti-hydrogen collaboration at the Large Hadron Collider in Switzerland uses radioactive ^{22}Na, which decays emitting high energy positrons as their positron source, while they take their antiprotons from the Antiproton Decelerator there.

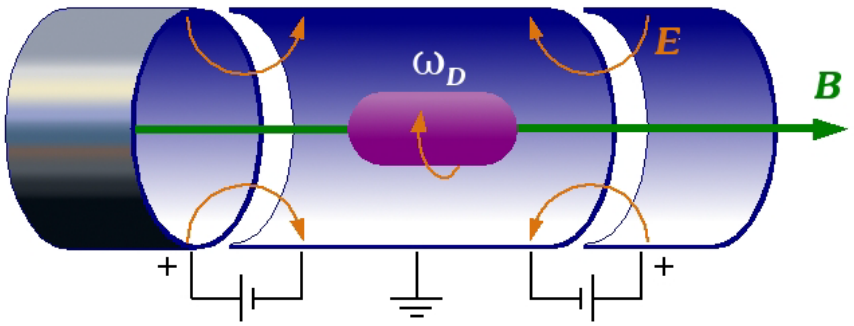

Figure 1.1 General design of the Malmberg-Penning trap

The Malmberg-Penning trap is widely used to study non-neutral plasmas. First used to study electron plasmas in the mid 1970's, The trap is now used in a number of modern experiments, possibly most prestigious among them being the ALPHA collaboration creating anti-hydrogen at CERN. Briefly, the CERN experiment captures both positrons and electrons in the same trap, using a separate catch sequence to confine them, then combining them into anti-hydrogen.

1.3 ^7Be

The goal of the larger Ion Project at BYU is the measurement of the half life of ionized beryllium-7 (^7Be) to an accurate degree. This may seem somewhat esoteric, but an accurate measurement of ^7Be is both important and difficult to perform. ^7Be decays 100% of the time by electron capture β-decay. It usually decays through one of two mechanisms:

$$^7Be + e^- \rightarrow {}^7Li + \nu_e + 861.8\ keV \tag{1.1}$$

$$^7Be + e^- \rightarrow {}^7Li* + \nu_e + 384.2\ keV$$

$$^7Li* \rightarrow {}^7Li + \gamma + 477.6\ keV \tag{1.2}$$

The first reaction appears to occur in 89.6% of the reactions, while the remaining 10.4% of the reactions follow the second reaction cycle.

Because it decays by electron capture, ^7Be's decay rate is affected by the availability of electrons surrounding it. This is problematic because ^7Be usually occurs naturally in compounds, which will have different decay rates depending on the compound. Table 1.1 shows a number of measured ^7Be decay rates in different compounds, which range from as low as 52.47 days for ^7Be encased in a C_{60} buckyball to 54.226 days for BeO.

These differences in decay rates have theoretical consequences. In the sun, ^7Be is created in the proton-proton fusion cycle, and it's decay is used to probe the interior of stars, which in turn helps understand the fusion cycle. The Standard Solar Model (SSM) uses calculations of ^7Be decay and ^7Be, ^8B reactions in the model, which constitute a potentially significant source of uncertainty in the model [9]. A more accurate measurement of ^7Be electron capture decay will contribute to a higher accuracy for the SSM. As no known experiments have been made which measure the decay of ^7Be in any state of ionization, BYU's experiment is in a unique position to contribute to greater accuracy of the SSM.

Recent models created using Harttree-Fock self consistent field and Density Functional Theory methods at BYU suggest a large gap between the decay rates of neutral ^7Be and ^7Be in the various compounds within which it has been measured to date [10]. Should BYU succeed in measuring the half-life of $^7Be^+$ in laboratory conditions, extrapolating that rate to a neutral ^7Be rate should be easily done.

1.4 Berstein Modes

I. B. Bernstein first predicted his namesake's wave in a groundbreaking theoretical paper in 1958 [11]. In this work, Bernstein postulated undamped radial oscillations of a quasi-neutral plasma

Table 1.1 Some of the measured values of the half-life of ^{7}Be under varying conditions.

Environment	**$T_{1/2}$ (days)**	**$\Delta T_{1/2}$ (days)**
"Accepted value"	53.22	0.06
BeO [a]	54.226	0.006
$Be^{2+}(OH_2)_4$ [a]	53.694	0.006
BeO, BeF_2, $Be(C_5H_5)_2$ (average) [b]	53.52	0.05
$Be(OH)_2$ [a]	53.416	0.006
Be [c]	53.376	0.016
Au [d]	53.311	0.042
Be (annealed metal) [f]	53.25	0.04
Al [f]	53.17	0.07
Be (annealed metal) [h]	53.12	0.06
LiF [h]	53.12	0.07
Al_2O_3 [i]	52.927	0.056
C_{60} (endohedral) [g]	52.68	0.05
C_{60} (endohedral, T=5 K) [j]	52.47	0.04

[a] Chih-An Huh, Earth Planet. Sci. Lett. **171**, 325-328 (1999).

[b] H. W. Johlige, *et al.*, Phys. Rev. C **2**(5), 1616-1622 (1970).

[c] Zhi-Yi Liu, *et al.*, Chin. Phys. Lett. **20**(6), 829 (2003).

[d] E. B. Norman, *et al.*, Phys. Lett. B **519**, 15-22 (2001).

[e] T. Ohtsuki, *et al.*, Mater. Trans. **48**(4), 646-648 (2007).

[f] F. Lagoutine, *et al.*, Int. J. Appl. Radiat. Isot. **26**, 131-135 (1975).

[g] T. Ohtsuki, *et al.*, Phys. Rev. Lett. **93**(11), 112501 (2004).

[h] M. Jaeger, *et al.*, Phys. Rev. C **54**(1), 423-424 (1996).

[i] A. Ray, *et al.*, Phys. Lett. B **455**, 69-76 (1999).

[j] T. Ohtsuki, *et al.*, Phys. Rev. Lett. **98**(25), 252501 (2007).

in a radially symmetric magnetic field. According to his work, these oscillations should be found near, but not exactly at, the cyclotron frequency of any plasma if properly stimulated. These results were subsequently confirmed in neutral plasmas the mid 1960s [12], and more recently have been confirmed in electron non-neutral plasmas [13].

1.4.1 Derivation of Bernstein Modes

Bernstein modes can be solved for linearly, but are some of the most difficult modes to derive in plasma physics. Many plasma oscillations, including the dispersion relations for Ion acoustic waves, Ordinary and extraordinary waves, and Alfen and whistler waves, can be derived using the MHD equations for plasmas. These derivations assume one can ignore single particle motions and only deal with collective motions of the particles. Bernstein modes, however, do not appear with such generalizations; to find them, one must resort to using the equations of kinetic theory, of which the MHD equations are a moment.

The fundamental equation in kinetic theory is the Boltzmann equation:

$$\frac{\partial f}{\partial t} + \mathbf{v} \cdot \nabla f + \frac{\mathbf{F}}{m} \cdot \frac{\partial f}{\partial \mathbf{v}} = \left(\frac{\partial f}{\partial t} \right)_c . \tag{1.3}$$

If a plasma is hot enough and we assume only electromagnetic forces, that equation can be written:

$$\frac{\partial f}{\partial t} + \mathbf{v} \cdot \nabla f + \frac{q}{m} (\mathbf{E} + \mathbf{v} \times \mathbf{B}) \cdot \frac{\partial f}{\partial \mathbf{v}} = 0. \tag{1.4}$$

Linearizing this equation with the assumption that the base electric field $E_0 = 0$, we get:

$$\frac{\partial f_1}{\partial t} + \mathbf{v} \cdot \nabla f_1 + \frac{q}{m} (\mathbf{v} \times \mathbf{B}_0) \cdot \frac{\partial f_1}{\partial \mathbf{v}} = -\frac{q}{m} (\mathbf{E}_1 + \mathbf{v} \times \mathbf{B}_1) \cdot \frac{\partial f_0}{\partial \mathbf{v}} \tag{1.5}$$

Assuming solutions for the perturbed wave function $f_1(\mathbf{r}, \mathbf{v}, t)$ are maxwellian, one can perform

fourier analysis on equation 1.5, which will yield solutions that can be written in the form of the plasma dielectric tensor ε. These elements can be written:

$$\begin{aligned}
\varepsilon_{xx} &= 1+\sum_s \frac{\omega_{ps}^2}{\omega^2}\frac{e^{-b_s}}{b_s}\zeta_{0s}\sum_{-\infty}^{\infty} n^2 I_n(b_s)Z(\zeta_{ns}) \\
\varepsilon_{yy} &= 1+\sum_s \frac{\omega_{ps}^2}{\omega^2}\frac{e^{-b_s}}{b_s}\zeta_{0s}\sum_{-\infty}^{\infty} \left\{n^2 I_n(b_s)+2b_s^2[I_n(b_s)-I_n'(b_s)]\right\}Z(\zeta_{ns}) \\
\varepsilon_{zz} &= 1+\sum_s \frac{\omega_{ps}^2}{\omega^2}\frac{e^{-b_s}}{b_s}\zeta_{0s}\sum_{-\infty}^{\infty} I_n(b_s)\zeta_{ns}Z'(\zeta_{ns}) \\
\\
\varepsilon_{xy} &= -\varepsilon_{yx} = i\sum_s \pm\frac{\omega_{ps}^2}{\omega^2}e^{-b_s}\zeta_{0s}\sum_{-\infty}^{\infty} n[I_n(b_s)-I_n'(b_s)]Z(\zeta_{ns}) \\
\varepsilon_{xz} &= \varepsilon_{zx} = \sum_s \pm\frac{\omega_{ps}^2}{\omega^2}\frac{e^{-b_s}}{(2b_s)^{1/2}}\zeta_{0s}\sum_{-\infty}^{\infty} nI_n(b_s)Z'(\zeta_{ns}) \\
\varepsilon_{yz} &= -\varepsilon_{zy} = i\sum_s \pm\frac{\omega_{ps}^2}{\omega^2}\left(\frac{b_s}{2}\right)^{1/2}e^{-b_s}\zeta_{0s}\sum_{-\infty}^{\infty}[I_n(b_s)-I_n'(b_s)]Z'(\zeta_{ns})
\end{aligned} \tag{1.6}$$

where the first summation is taken over each species of particle s, $I_n(b_s)$ is the n^{th} order Bessel function of imaginary argument, and the other parameters are defined as follows:

$$\begin{aligned}
Z(\zeta) &= \frac{1}{\pi^{1/2}}\int_{-\infty}^{\infty}\frac{e^{-s^2}}{s-\zeta}ds \\
\omega_{ps}^2 &= n_{0s}Z_s^2\frac{e^2}{\varepsilon_0 m_s} \\
\zeta_{ns} &= \frac{\omega+n\omega_{cs}}{k_z v_{ths}} \\
\zeta_{0s} &= \frac{\omega}{k_z v_{ths}} \\
\omega_{cs} &= \left|\frac{Z_s eB_0}{m_s}\right| \\
v_{ths}^2 &= \frac{2KT_s}{m_s} \\
b_s &= \frac{1}{2}k_\perp^2 r_{Ls}^2 = k_x^2\frac{KT_s}{m_s\omega_{cs}^2}
\end{aligned}$$

Bernstein waves will propagate perpendicular to B_0 at or near harmonics of the cyclotron frequency ω_c. By solving $\nabla\varepsilon\cdot\mathbf{E}=\mathbf{0}$ using these dielectric elements, the following dispersion relation results:

$$k_x^2\varepsilon_{xx}+2k_xk_z\varepsilon_{xz}+k_z^2\varepsilon_{zz}=0 \tag{1.7}$$

It can be shown that, when replacing the tensor elements with the definitions above, the following dispersion relation for Bernstein waves results.

$$1+\sum_s\frac{k_D^2}{k_\perp^2}e^{-b}\sum_{n=-\infty}^{\infty}I_n(b)\left[1-\frac{\zeta_0}{\zeta_n}\right]=0 \tag{1.8}$$

Where $k_D^2=\frac{2\omega_p^2}{v_{th}^2}$. This result makes use of the fact that $Z_n\approx-\frac{1}{\zeta_n}$ for large ζ. For a more robust treatment of Bernstein mode linear theory, please consult Chen, 1984 [14]. Note that this theory is valid only in an assumed infinite column of plasma. Differences will necessarily arise when working with the real plasmas present in the Ion Experiment. Most directly, the previous derivation rests on the assumption that the plasma is infinite, an infinite sheet or cylinder.

The mode we specifically wish to study with the Ion Experiment is an azimuthally symmetric mode, the $m=0$ Bernstein mode. This symmetry means that conventional means of measuring oscillations in such a plasma will not detect the mode. Most means of detecting oscillations in plasmas to date have used changing numbers of particles under segmented confinement rings to detect oscillations of their corresponding plasmas. This method will allow detection of non-uniform modes such as the Bernstein $m=1$ or $m=2$ mode.

To measure any symmetric mode, however, this technique will not work. The $m=0$ mode doesn't change the potential underneath the individual segments of a segmented ring, which renders the rings useless for detection of the oscillation. The position of the plasma in the Ion Experiment, as well as the setup of its rings, should allow for detection of the $m=0$ mode, which will be discussed in Chapter 2.

1.4.2 Brillouin Limit

Densities of non-neutral plasmas are limited by internal electrostatic repulsion of the plasma particles, given by the Brillouin Limit. Taking an infinite cylindrical plasma with a constant velocity, we can balance the forces in the radial direction:

$$\begin{aligned} \sum F &= m\frac{v^2}{r} \\ \Rightarrow qE_r - qv_\theta B_z &= -m\frac{v_\theta^2}{r} \end{aligned} \tag{1.9}$$

Solving poisson's equation in cylindrical coordinates, and remembering we have a plasma with uniform azimuthal velocity, we get:

$$\begin{aligned} \frac{1}{r}\frac{\partial}{\partial r}\left(r\frac{\partial V}{\partial r}\right) &= \frac{nq}{\varepsilon_0} \\ \Rightarrow \frac{nqr^2}{2\varepsilon_0} &= r\frac{\partial V}{\partial r} \\ \Rightarrow \frac{nqr}{2\varepsilon_0} &= \frac{\partial V}{\partial r} = -E_r \end{aligned} \tag{1.10}$$

Utilizing equation 1.10 in equation 1.9, we obtain:

$$\begin{aligned} \frac{nq^2r}{2\varepsilon_0} - qv_\theta B_z &= -m\frac{v_\theta^2}{r} \\ \Rightarrow \omega_p^2\frac{r}{2} &= -\frac{v_\theta^2}{r} + \frac{qv_\theta B_z}{m} \\ \Rightarrow 0 &= \omega^2 - \omega\omega_c + \omega_p^2 \end{aligned} \tag{1.11}$$

where $\omega_p^2 = \frac{ne^2}{m\varepsilon_0}$ is the plasma frequency and $\omega_c^2 = \frac{e^2B^2}{m^2}$ is the cyclotron frequency. The solution to this quadratic is:

$$\omega = \frac{\omega_c}{2}\left(1 \pm \sqrt{1 - 2\frac{\omega_p^2}{\omega_c^2}}\right) \tag{1.12}$$

To have a real solution, the value under the radical must be greater than or equal to zero, implying:

$$2\omega_p^2 \leq \omega_c^2$$

Remembering the definition of ω_p, we can solve for the maximum possible number density, which yields:

$$n \leq \frac{B^2 \varepsilon_0}{2m}. \tag{1.13}$$

This equation constitutes the Brillouin Density Limit for a non-neutral plasma. Bernstein modes can only be detected when the density of the plasma is near this limit - in all other situations, the oscillations will be too small to measure. This derivation has assumed an infinite plasma with a constant density, but it has been shown that the Brillouin limit still holds in cases of non uniform density and non-infinite plasmas [15].

Chapter 2

The Ion Experiment

The Ion Experiment at BYU is a Malmberg-Penning trap. The experiment consists of a metal vacuum vapor arc (MeVVA) source coupled with a high voltage bias and extractor grid, a quadrupole magnet used to filter contaminating ions from the plasma, and set of confinement rings separately connected to their own voltage sources. The rings are surrounded by a solenoid electromagnet to provide axial confinement. Diagnostics for the experiment include a non-destructive FT-ICR system and destructive charge collecting rings. To increase confinement time, the experiment includes a rotating wall, similar to the wall used in the UCSD ion experiment.

2.1 MeVVA Source

The MeVVA source consists of a trigger circuit, a removable cathode assembly, and a a set of mounting rings. Each of these pieces will briefly be explained. More detail is available in David Olson's Masters Thesis [16].

The trigger circuit contains a pulse transformer designed to yield a maximum of 8 kV, .5 μs low current output arc. The transformer triggers an air spark gap, which consists of two spherical electrodes and a trigger electrode. The electrode, in turn, discharges a high voltage capacitor

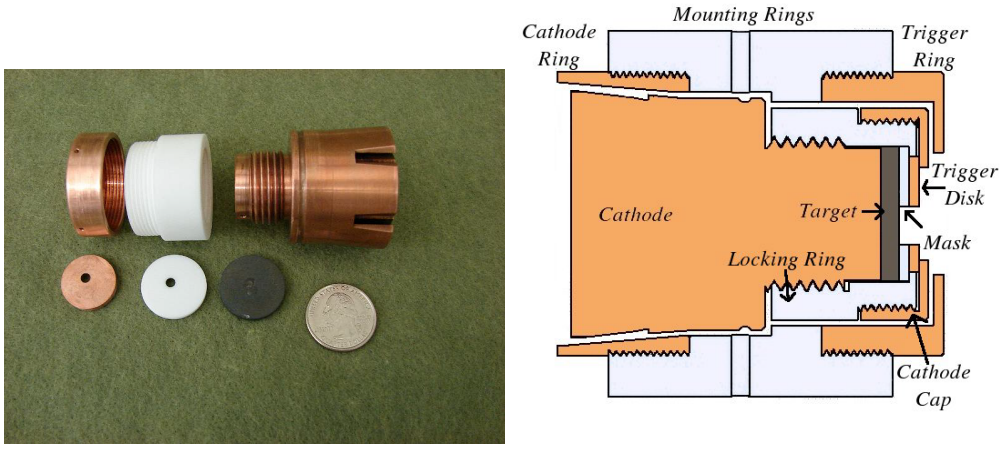

Figure 2.1 The MeVVA source

through a step up transformer, which discharges to the ion source.

The ion source is held in a removable cathode assembly (figure 2.1). This assembly consists of a base, a locking ring, a target mask, trigger disk and ion source, and a cap. The cap, trigger disk, and cathode base are made of OFHC (oxygen-free high conductivity) copper.

The geometry of the cathode assembly is cylindrical, first to ensure good electrical contact between the movable cathode assembly and the mounting rings, and second, to hold the cylindrical ion source, which is currently a boron-carbide wafer. The locking ring, made of Macor, is threaded on the back end to match the threading on the base, and threaded on the front to match the threading of the trigger ring. This allows the source to hold the boron-carbide wafer and the Macor ring in place. The cap is also threaded and maintains electrical contact with the trigger disk while holding the disk in place. The whole assembly is removable to facilitate quick removal of the source when it needs to be replaced.

The mounting rings sit inside the experimental structure, allowing for electrical contact. The mounting rings consist of a cathode, mounting, and trigger ring, and are held in place by a two-piece mounting bracket, which in turn held in place by screws.

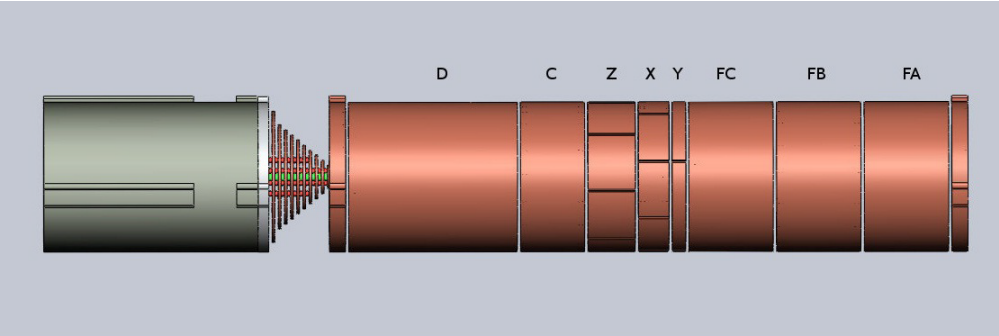

Figure 2.2 The BYU Ion Apparatus

2.2 The Trap

After firing the source, the quadrupole magnet removes contaminants, and the plasma is caught in the Malmberg-Penning trap. The trap is a collection of concentric OFHC copper rings with a standard radius of 4 cm, held together by threaded stainless-steel rods, plastic beads, and copper end brackets. There are 8 rings total: 3 fill rings and 5 confinement rings.

The fill rings, labeled Fill A (FA), Fill B (FB), and Fill C (FC), have lengths of 5 cm apiece, and line, from the ring closest to the source, FA, FB, then FC. The fill rings are used as a barrier to prevent leakage of the plasma toward the source during trapping and confinement. Following the fill rings are the confinement rings, named for historical reasons as X, Y, Z, C, and D. First from the direction of the source is the Y ring, which is 1 cm long and segmented into 4 sections for use with the Rotating Wall. Next is the X ring segmented into 8 sections for use with the Rotating Wall, and is 2 cm long. Finally we have the Z ring, at 3 cm long, segmented into 8 sections for use with the FT-ICR diagnostics. The C ring is not segmented, and is 4 cm long. The segmented rings and the C ring are the main rings used for measuring potentials in the FT-ICR and driving the rotating wall. Following the C ring is the D (dump) ring, a ring used during the fill to keep plasmas from leaking toward the CC (charge collector) disks.

Each of the rings in the trap are connected via coaxial cables to BNC connectors from which

potentials can be monitored and adjusted as the need arises. In addition to setting the potentials on the rings, these BNC cables drive the rotating wall and look for frequencies with the FT-ICR. The cables connect to a network of timing boxes, which are in turn to a computer, which runs the experiment. The timing of the experiment is controlled by an FPGA.

Providing confinement along the axis of our experiment is an electromagnet with a maximum field of .45 Tesla.

2.3 Diagnostics

Multiple diagnostic techniques are available on the Ion Experiment. Most relevant to our discussion are the FT-ICR and the CC disks. FT-ICR is a mass spectrometry technique used to discover the type and number of particles in a penning trap. The technique searches for resonances close to the ion cyclotron frequency, then using the relationship $\omega_c = \frac{eB}{m}$, and with a well-known magnetic field, one can discover the ratio $\frac{e}{m}$, and by so doing find the mass of the particles in the machine, thereby finding which particles are there. At BYU, the FT-ICR have also been used to search for diocotron modes to search for the presence of any ions at all.

The disks are a set of 10 concentric copper plates at the end of the ion experiment of varying radii (figure 2.3, all of which are connected by BNC cable to the integrators near the experiment and ultimately to the computer. After holding a plasma for a period, the potential on the D ring can be dropped and ions will be forced by the still present potential on the fill rings to flow out of the trap and onto these plates. Measuring the potential on these rings through the integrator will give the total number of charges that hit these rings. Dividing the number of charges that hit a ring by the exposed area of that ring will give a single ring density. Each ring is connected to its own integrator, all of which have been calibrated so as to find the correct number of charges for each dump. Viewing the data of each ring gives a radial profile of the plasma present when the dump

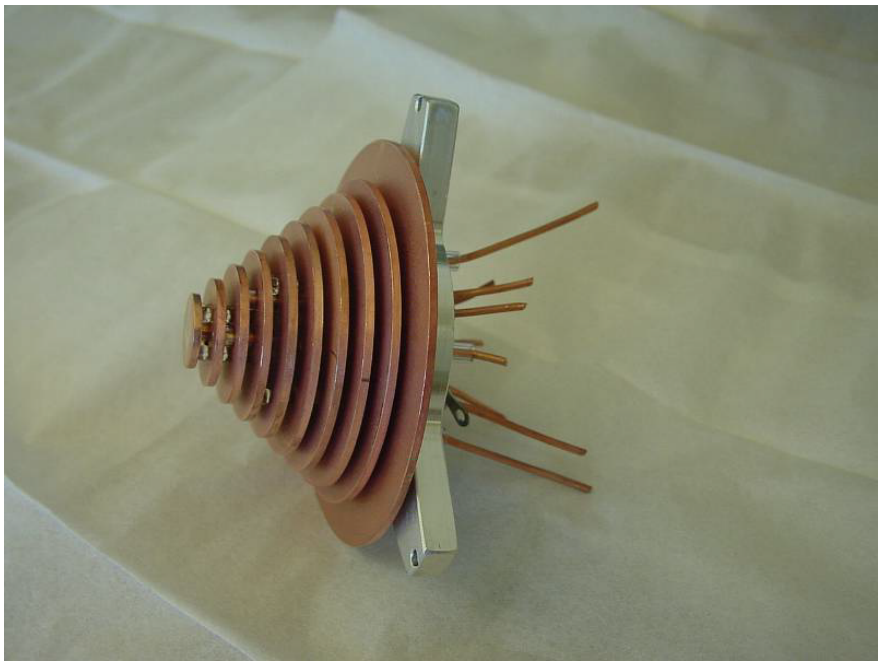

Figure 2.3 The Charge Collecting Rings

occurred, and through MATLAB fitting techniques the central charge density of the plasma as well as the numbers of present electrons and ions can be found.

2.4 Measuring Bernstein Modes

Catching of a plasma occurs in the following sequence: First, the source is fired, arcing to the wafer of boron carbide and freeing ions which are then pushed toward the Penning trap using a high negative potential. During the firing sequence the D ring will be held at a +150 V potential, providing a wall to hold the ions in the trap. Timing is set up such that fill ring FA will rise to +150 V, following which fill FB will do the same. As some electrons can be caught in the trap with the ions, various sequences are used to remove the electrons, and the experiment should be filled with a one species plasma.

The now captured ions can be excited to measure the Bernstein modes present in the plasma.

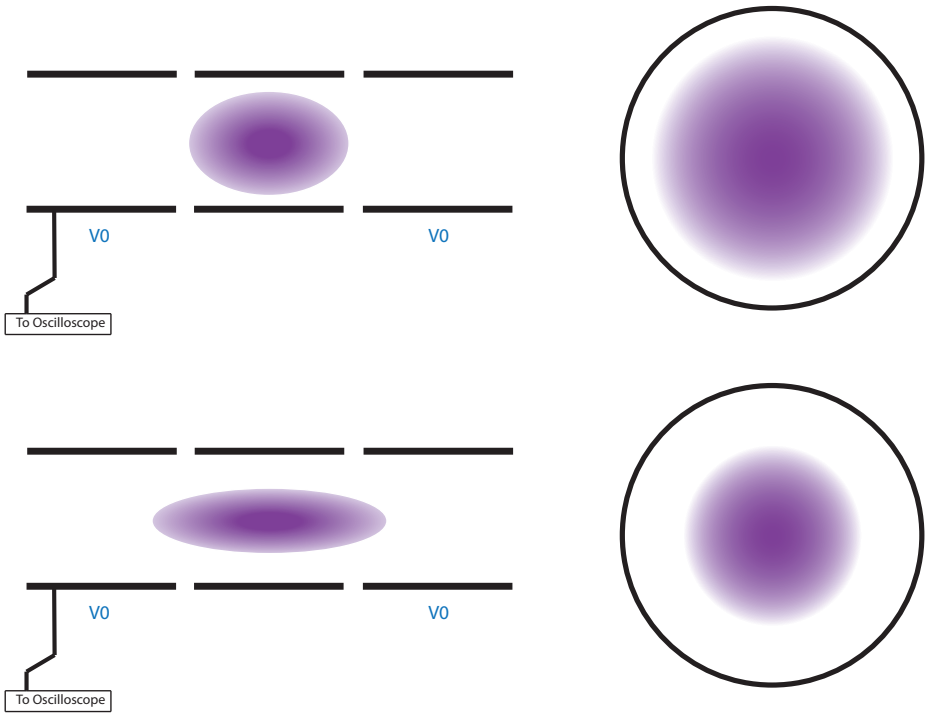

Figure 2.4 Illustration of Bernstein oscillations from the side and end. A potential is applied to the outer ring, which forces the ends of the plasma to oscillate along the cylinder's axis. This thereby causes the plasma to oscillate radially.

A small oscillating potential is applied to the fill rings FA and FB and the dump ring near the theoretical cyclotron frequency of the plasma, which should force the ions to oscillate parallel to the magnetic field and perpendicular to the end potentials. This process is pictured in figure 2.4.

As mentioned in the introduction, $m = 0$ Bernstein modes cannot be measured conventionally. Our experimental setup, however, provides a way to measure that particular mode. The theoretical Bernstein modes mentioned in the introduction are derived with the assumption of an infinite cylinder of plasma, but our experimental plasma is not infinite. As it is finite, modes that oscillate perpendicular to the magnetic field will force the ends of the plasma to oscillate parallel to the field as well. This parallel oscillation can be measured.

Previous measurements of the plasma have suggested that the plasma should be located under-

neath the X, Z, and C rings. As such, the forced plasma should oscillate underneath the C ring. This oscillation will change the potential under the ring periodically and allow measurement of that oscillation. The oscillation is measured using an oscilloscope, and the oscilloscope traces are saved using a LabVIEW code. After the traces are saved the data is read into MATLAB and using built-in fourier transform algorithms the power spectrum of the oscillating potentials can be obtained. The LabVIEW code is included in the appendix. To see the MATLAB code, please consult the BYU Plasma Group.

Currently, work is being done on a computational model of these finite length Bernstein modes. Having obtained data on existing modes, these modes can be compared with the computational model to compare our experiment with theory.

Chapter 3

Results

As of the writing of this thesis, we have been unable to take Bernstein mode data. Although the factors that contribute to our difficulties are not entirely clear, we feel that this difficulty is largely due to inconsistency in densities of and catch times of our plasmas. Our current boron-carbide plasma consists of about 80% boron and 20% carbon.

3.1 Timing

When originally designed, the source was set up to create a maximum-current arc in a short period of time. This configuration was chosen particularly to minimize the use of ^7Be when performing the experiment. Such short arc times do minimize use of ^7Be, but they also require intricate timing when raising the rings and consistent plasmas.

The timing rests on knowing when the plasma will arc and when that arc will produce the ions needed to trap. To maximize the arc over the course of the experiment, timing has been adjusted in various ways. When catching the plasma, the raise sequence of the D ring needs to be timed correctly to catch the slow-moving protons while allowing quicker moving electrons to drop out of the trap.

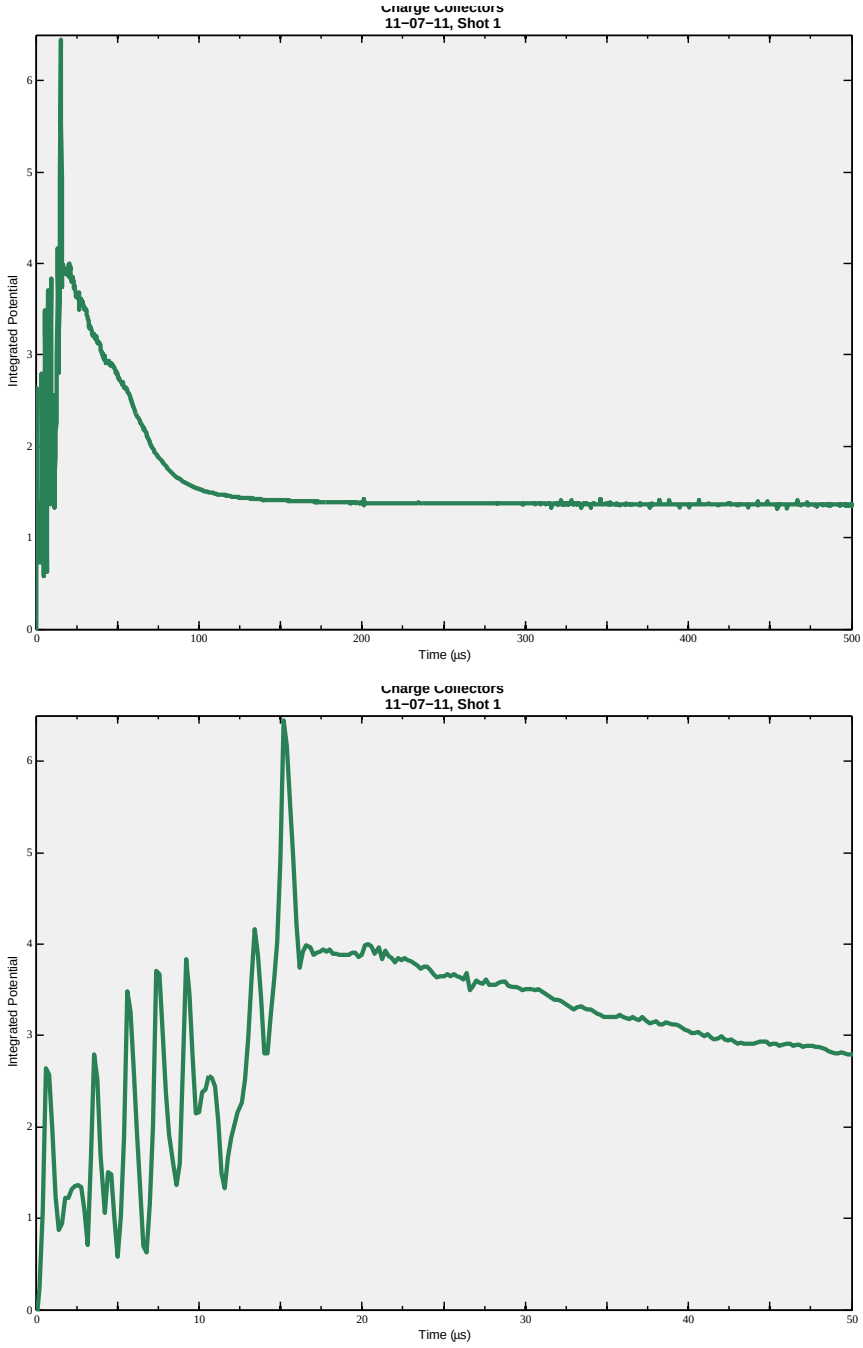

Figure 3.1 Trace during the fill sequence. This trace appeared to have a high density of ions..

One can find the time the plasma begins exiting the source by looking at a trace of the number of charges on the charge collecting rings as a function of time. Figure 3.1 gives a plot of this potential for an unusually good stack. The large "bump" in the plot likely indicates a large number of positive charges that have been liberated from the source. The plot shows the ions begin leaving the source somewhere between 15 and 17 μs after the source is fired. We calibrate the timing of the shot to catch the maximum possible number of charges, and so will time our raising of the D Ring at about 15 μs if this trace were typical of all traces.

These traces haven't been consistent, however. Figures 3.2 and 3.3 show two other charge collector traces with differing stack times. These sporadic arc times are confirmed by data from the source during the arc. Figure 3.4 shows data taken from our monitor at the source during firing. The plots are calibrated such that the arc begins at 0 on the plots. The oscillations in the plots can be explained as feedback from the circuits in the source itself. These traces show that the differing arc times are intrinsic to the system.

3.2 Plasma Density

In any plasma we catch, Bernstein modes are invisible unless we reach high densities; these densities need to be a substantial fraction of the Brillouin limit in order to be measured. According to equation 1.13, the Brillouin limit for a boron plasma is $5.13 \times 10^{13}\ m^{-3}$. Our plasmas have yet to reach densities close enough to the Brillouin limit to allow measurement of the Bernstein modes.

Figure 3.5 shows typical profiles of our plasma when dumped. As is clear, the line integrated density is around $n = 1.4 \times 10^{10}\ m^{-2}$. Previous measurements have suggested that our plasma is no shorter than 2 cm at the shortest, so taking this as the length of our plasma, we get densities of only $n \approx 7 \times 10^{11}\ m^{-3}$. Even in this best case scenario, the ratio of our plasma density to the Brillouin density limit is no better than $\frac{n}{n_B} \approx .014$, two orders of magnitude smaller than the limit.

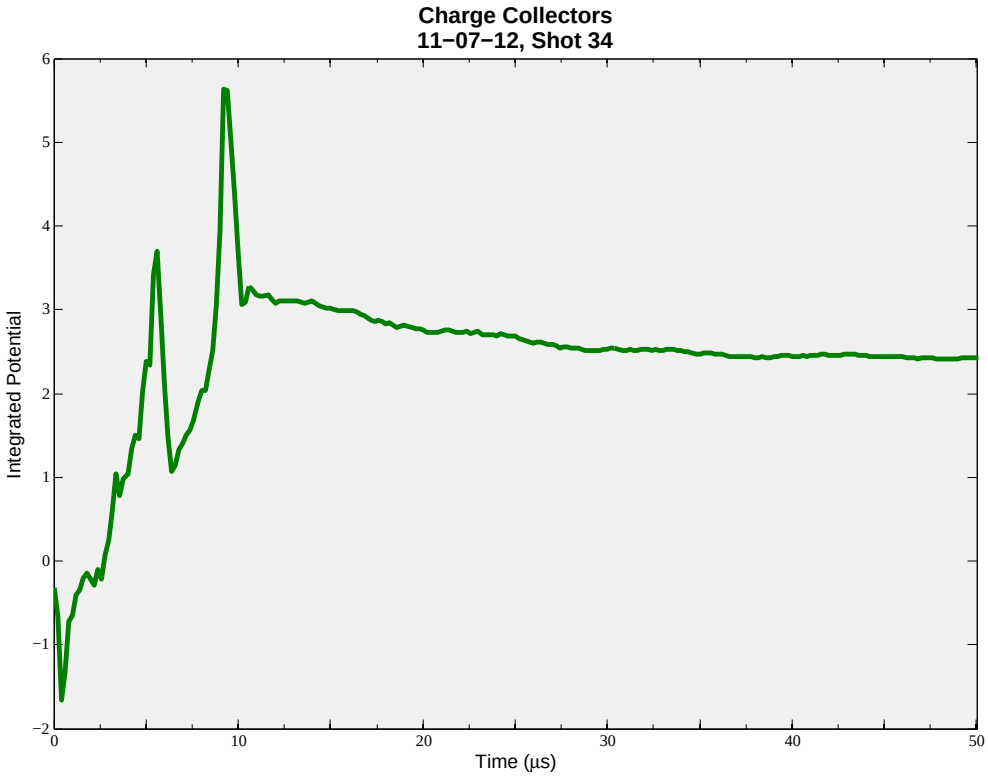

Figure 3.2 This plasma arc takes around 10 μs.

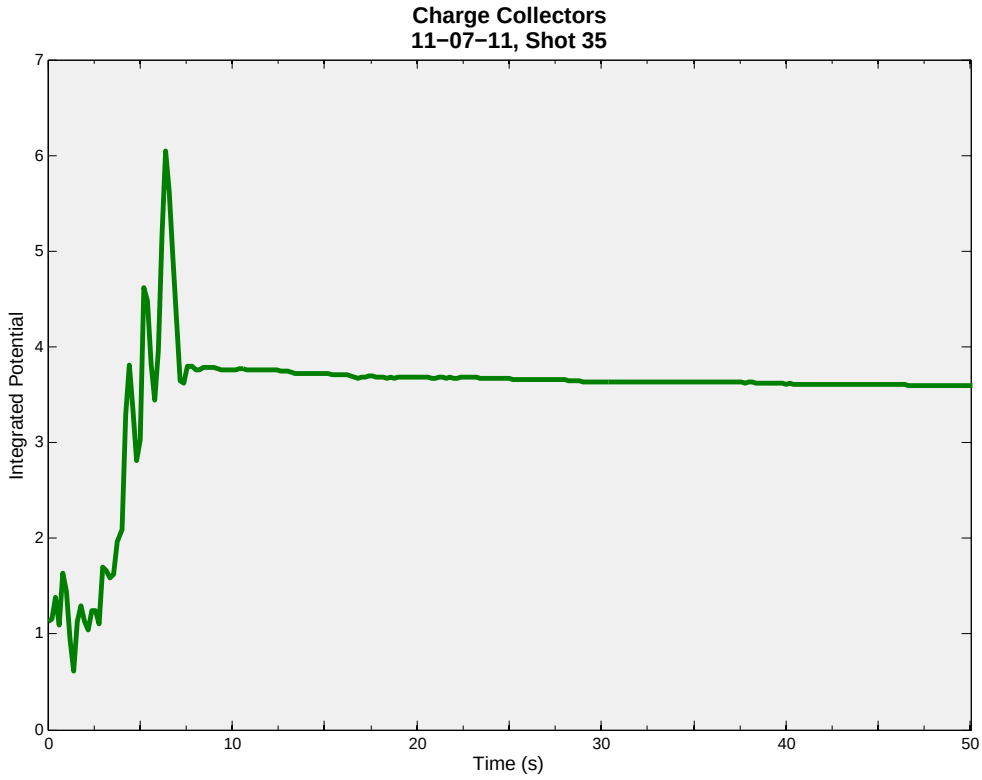

Figure 3.3 This plasma arc takes around 7 μs.

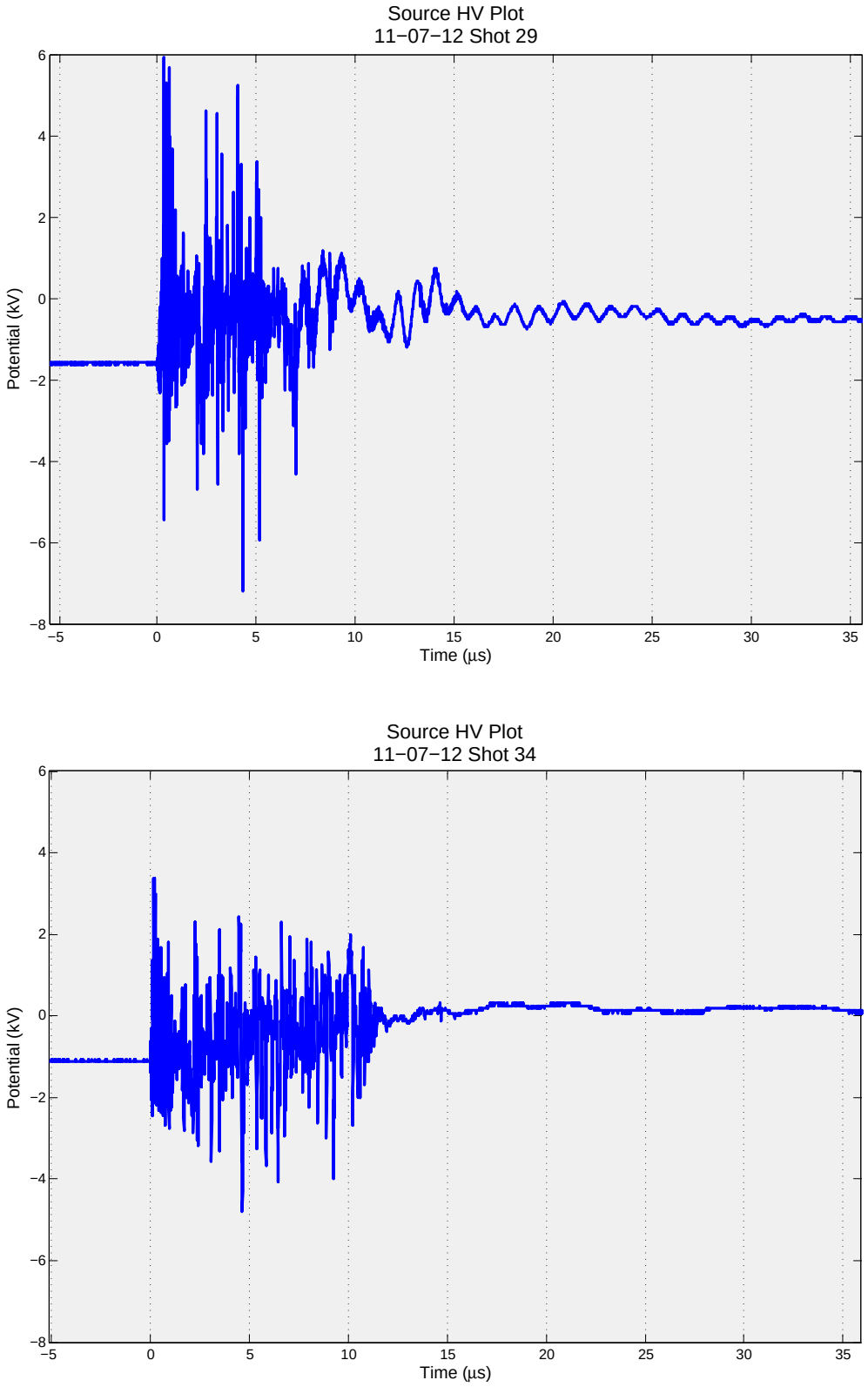

Figure 3.4 Two source traces. The traces show a wide range of arc times, from a little more than 5μs to nearly 15μs.

It is likely that at these densities the plasma oscillations will not be measurable.

Problematically, our plasma densities are not consistent enough to warrant even these high plasma density studies. While our plasmas have occasionally yielded densities high enough to warrant some optimism, generally even plasmas that have densities two orders of magnitude lower than the Brillouin limit are rare. Typically we get plasma line integrated densities in the 10^8 range at best, much smaller than the levels that we need for measurement. These measurements are sometimes small enough to be difficult to distinguish from noise in our charge collecting rings. In order to adequately measure the Bernstein modes, higher densities and better densities must be achieved.

3.3 Pulse Forming Network

To increase the density of our plasmas, we intend to modify the circuitry which generates our MeVVA arc. The modification we intend to make is in the form of a pulse-forming network (PFN). If successful, the addition of this network should lengthen the time of the arc while forcing out larger numbers of ions, and models of this network tested in our group suggest that this goal will be achieved.

The PFN is a network of high voltage capacitors connected to a network of inductors shown in figure 3.6. The network can be modeled simply using kirchhoff's laws

$$rI_1 + \frac{Q_1}{C} - \frac{Q_2}{C} + L_1\frac{dI_1}{dt} = 0 \tag{3.1}$$

$$rI_2 + \frac{Q_2}{C} - \frac{Q_3}{C} + L_2\frac{dI_2}{dt} = 0 \tag{3.2}$$

$$rI_3 + RI_3 + \frac{Q_3}{C} + L_3\frac{dI_3}{dt} = 0 \tag{3.3}$$

where r is the internal resistance of each inductor, R is the load resistance, and L_n is the inductance at each inductor. Current I_3 will exit to the load, which will in turn increase the length of the

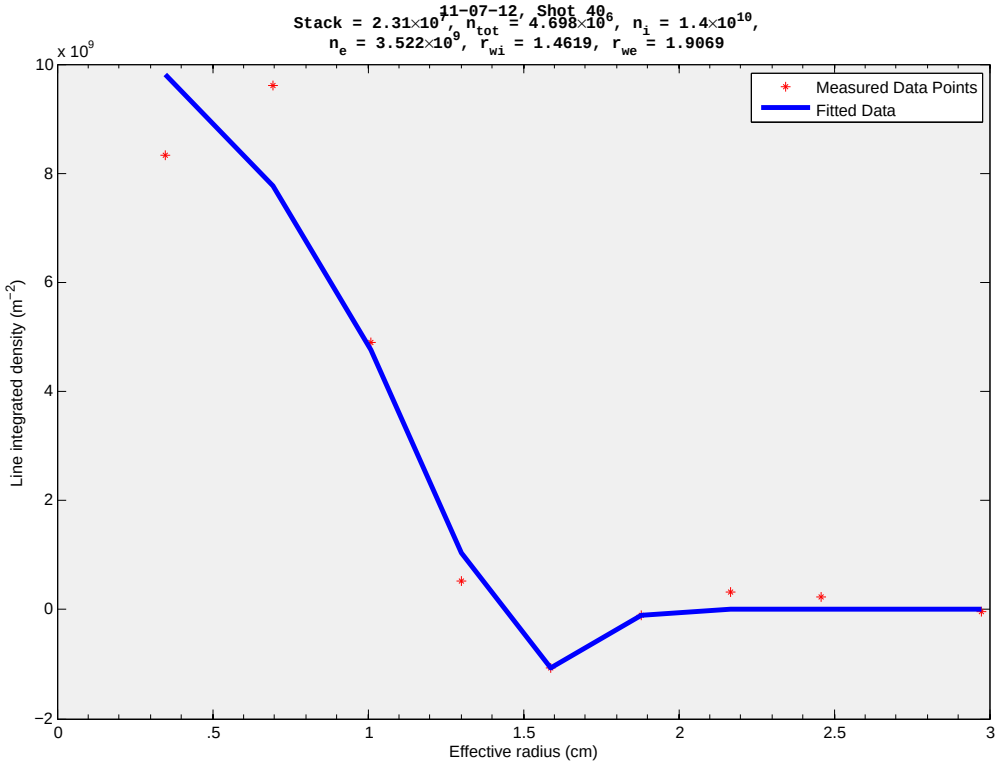

Figure 3.5 A typical trace of the dump sequence. This sequence shows a line integrated ion density on the order of 10^{10} m^{-2}, which is about the highest of the densities we have been able to achieve. These densities are likely too much smaller than the Brillouin limit to be detectable with our equipment.

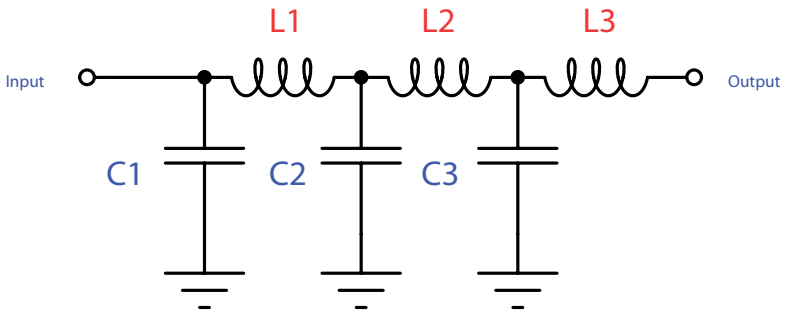

Figure 3.6 Pulse Forming Network Circuit Diagram.

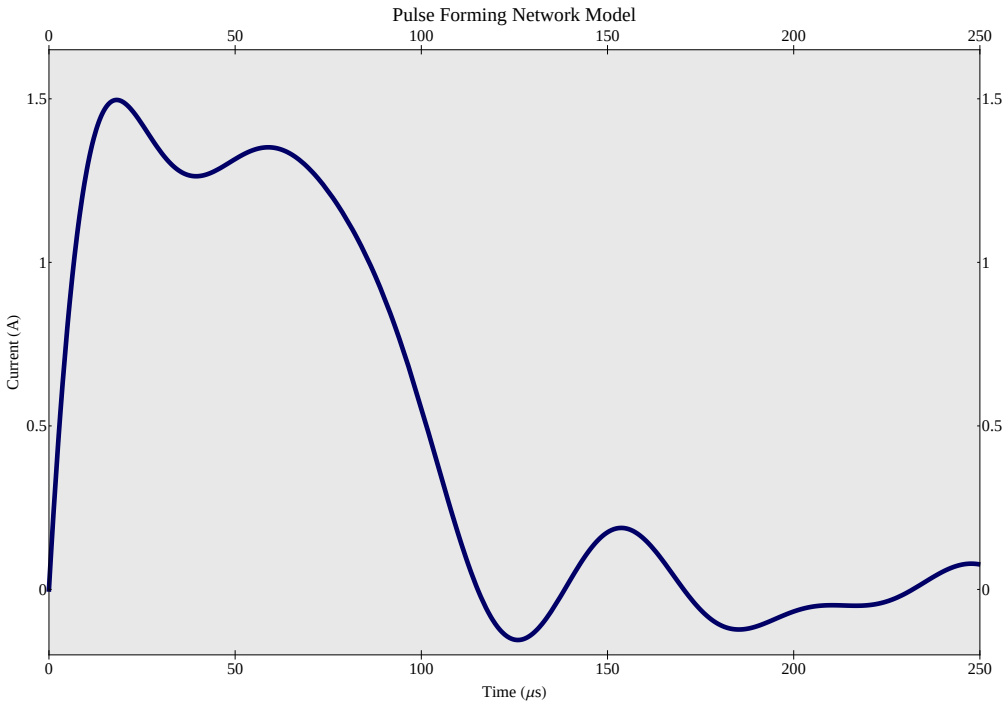

Figure 3.7 Model for the pulse forming network. The setup should create an arc of longer than 60 μs.

arc.

Our network has 3 inductors of 2000 μH inductance, and 3 capacitors of (.1) μF capacitance rated at 6 kV. The inductors are placed next to each other in such a way that the mutual inductance of the network brings the total inductance to 7500 μH. Modeling the network in Mathematica using the equations above, we obtain a pulse modeled by figure 3.7. According to the model, this design should increase the pulse length by 60 - 100 μs. The PFN has been placed in the source electronics as shown in the appendix.

3.4 Discussion and Conclusion

As of the publication of this thesis, we are still in the testing and integration phase of the PFN, but the models are promising. The longer arc time of the network should remove our problems

with arc time and density. The plan is to raise the D ring early, catching more plasma than we originally thought to catch. Doing this will allow for intermittent firing times, because the ring will be up long enough to compensate. This should also help with plasma densities, allowing the plasma to build up density over a longer period of time. These problems are left for future work on the apparatus, but must be solved to make Bernstein mode measurement, and indeed the ultimate goals of the Ion Experiment, possible.

Future work on the BYU Ion experiment will work on these problems. The PFN still has many issues to work out, but with luck and a little ingenuity, the experiment will soon have a working confined plasma with which we can measure ion Bernstein modes.

Appendix A

Circuit Diagrams and LabVIEW code

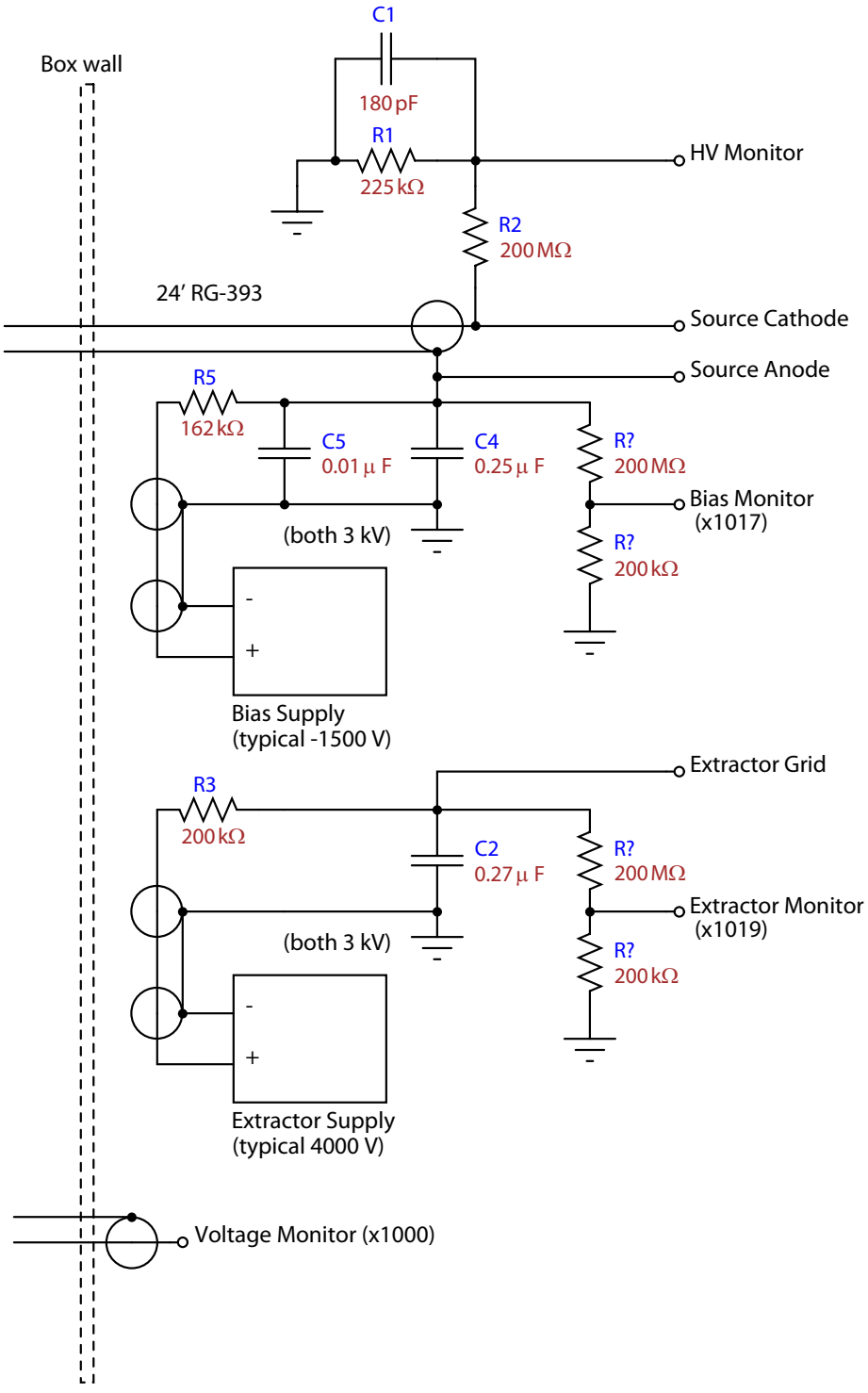

Figure A.1 MeVVA Supply before PFC

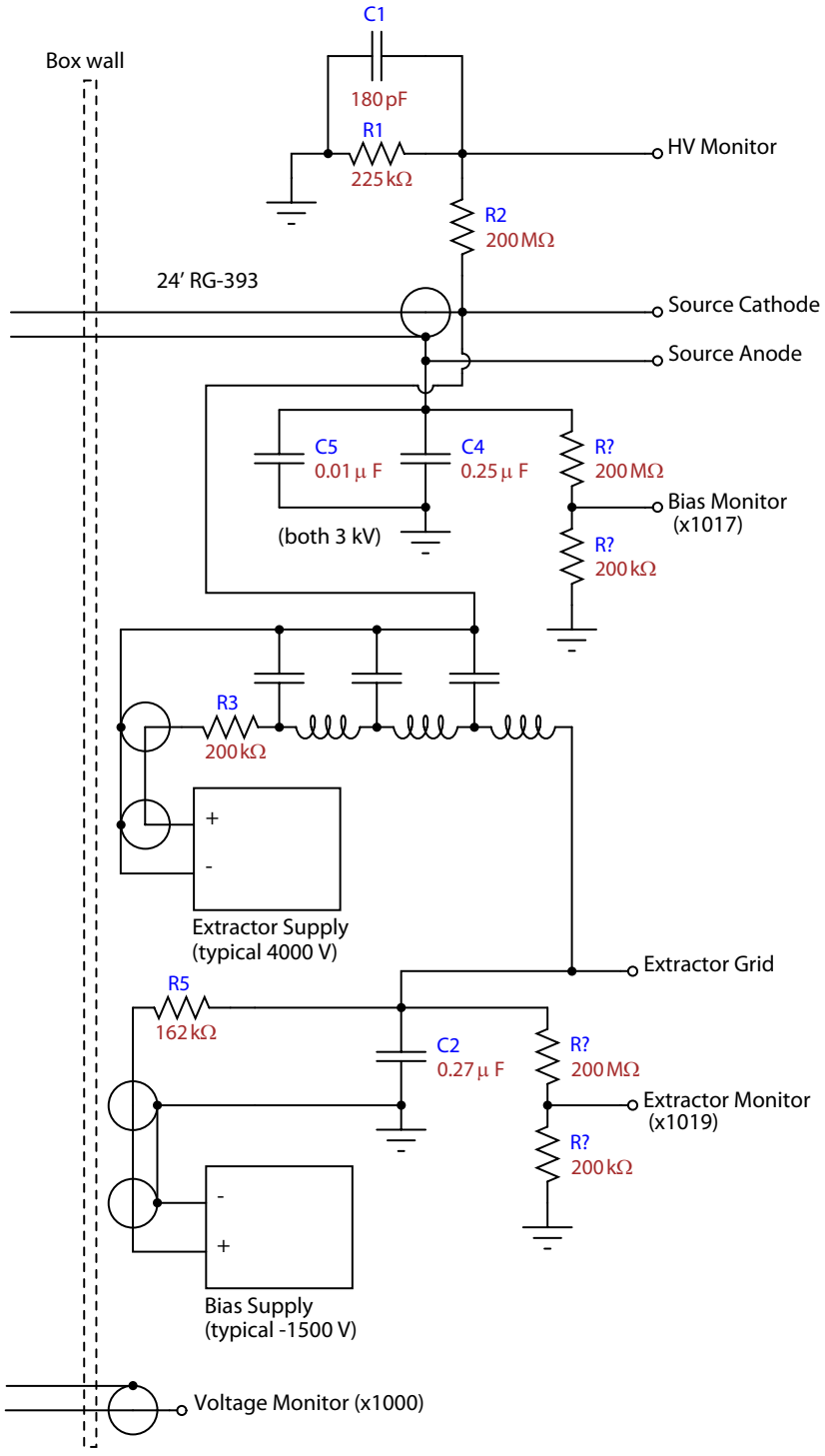

Figure A.2 MeVVA Supply after PFC

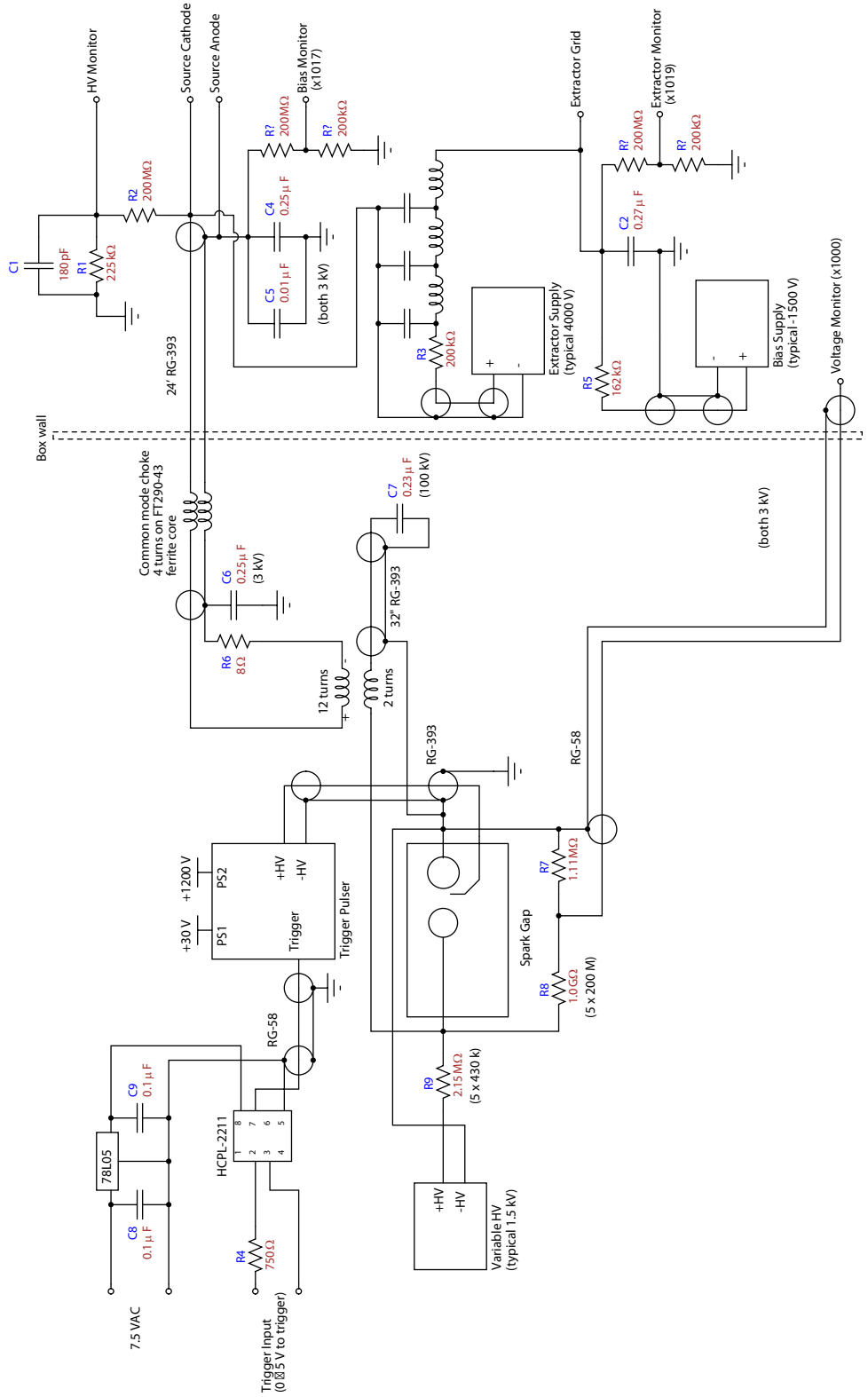

Figure A.3 MeVVA Full Circuit

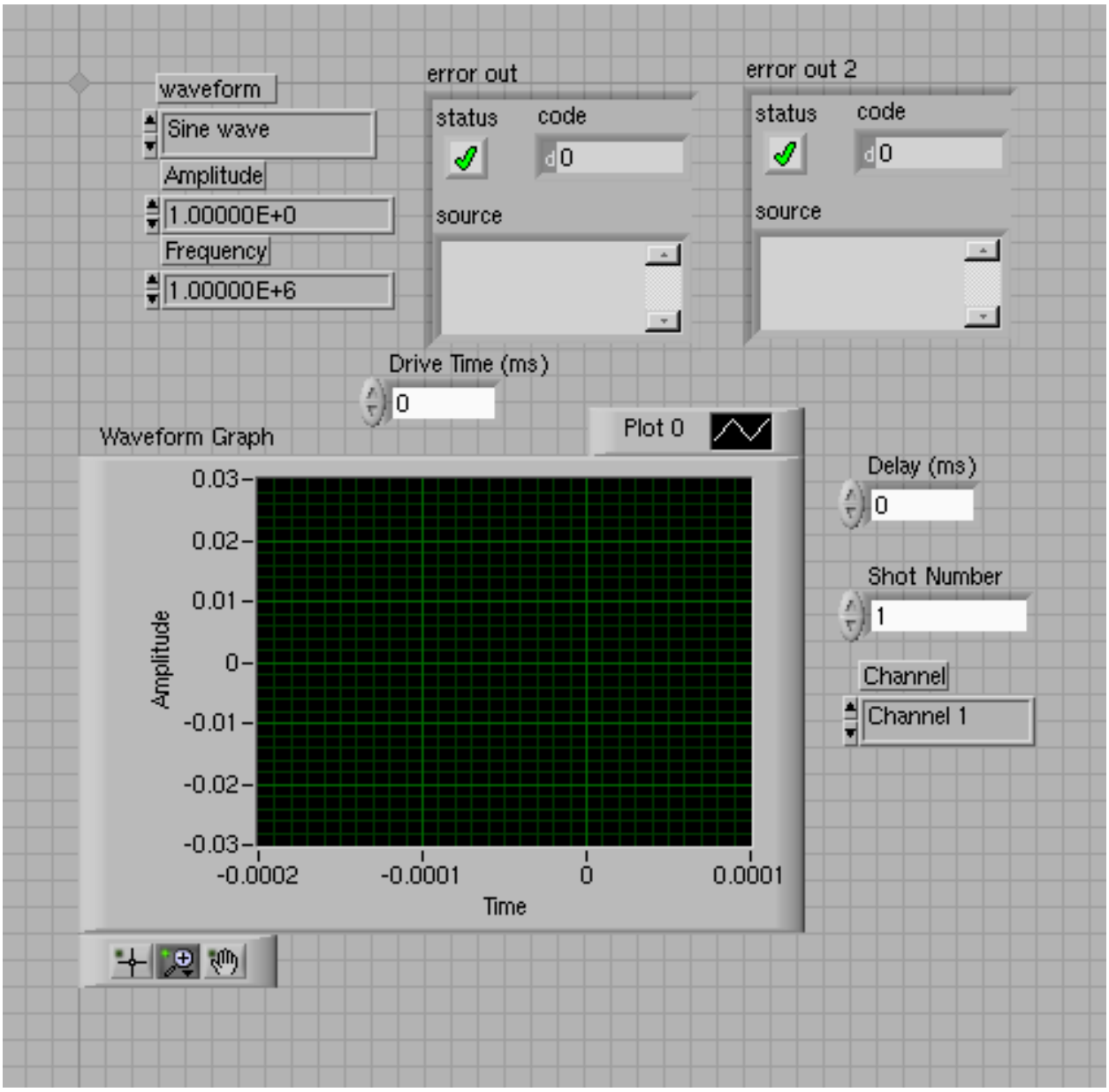

Figure A.4 Excite And Measure Mode.vi

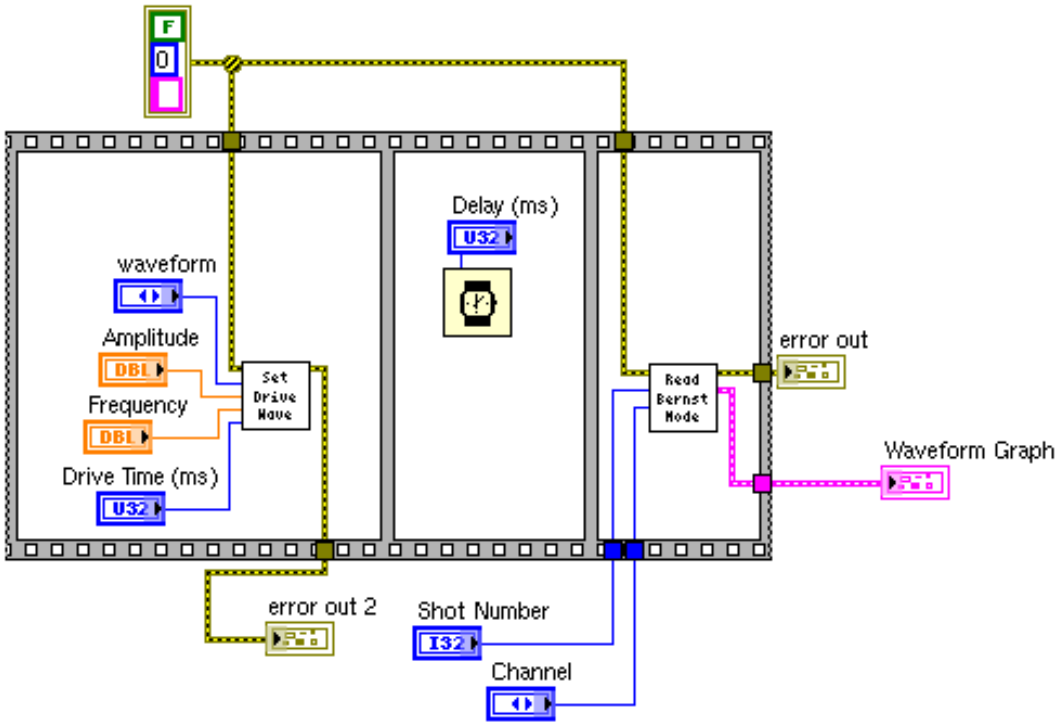

Figure A.5 Excite And Measure Mode.vi

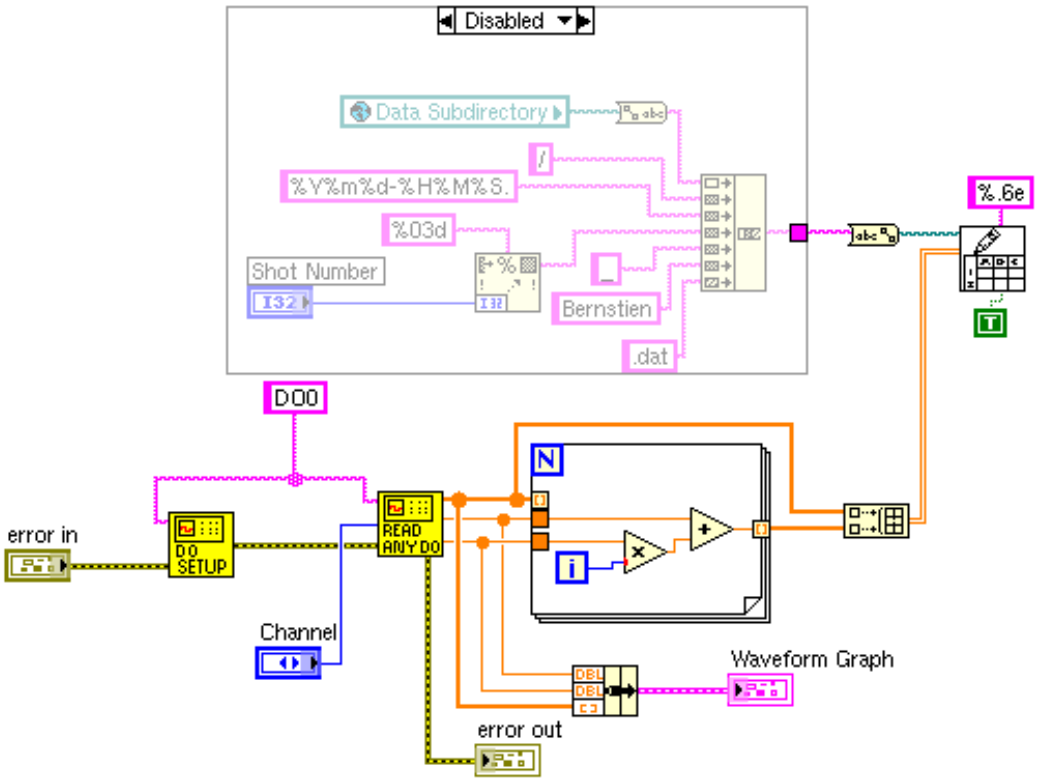

Figure A.6 Read Bernstein Mode.vi

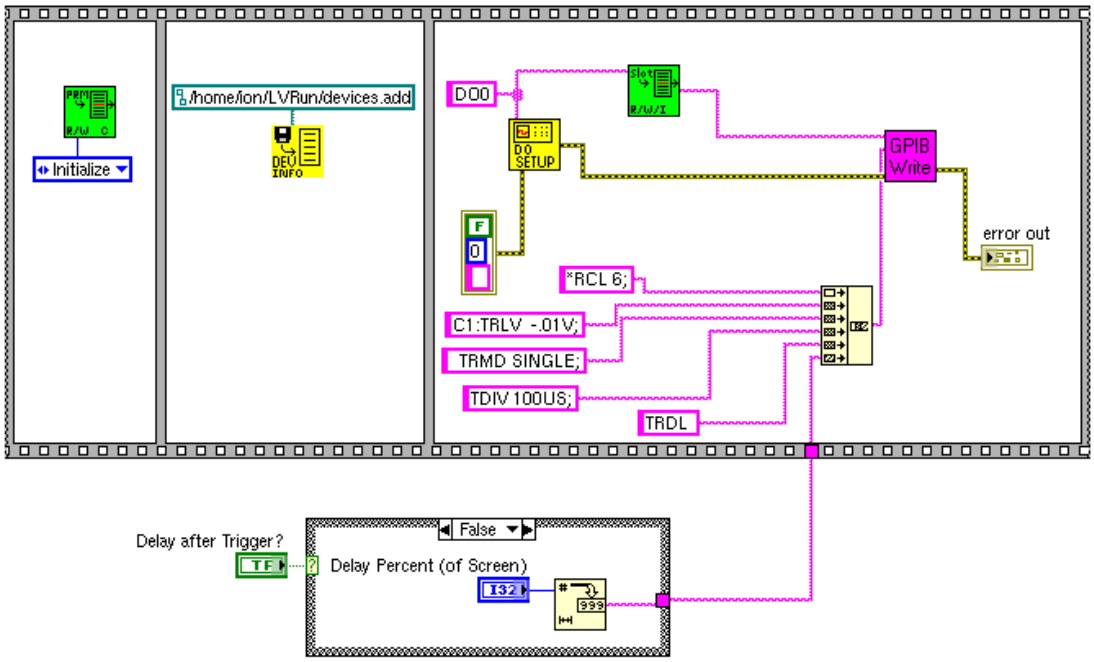

Figure A.7 Bernstein DO0 Setup.vi

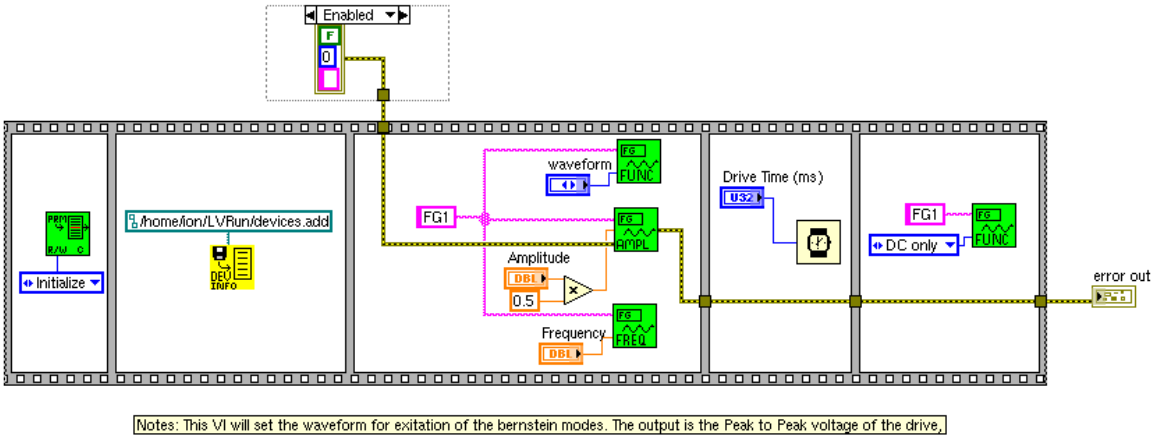

Figure A.8 SetWaveform.vi

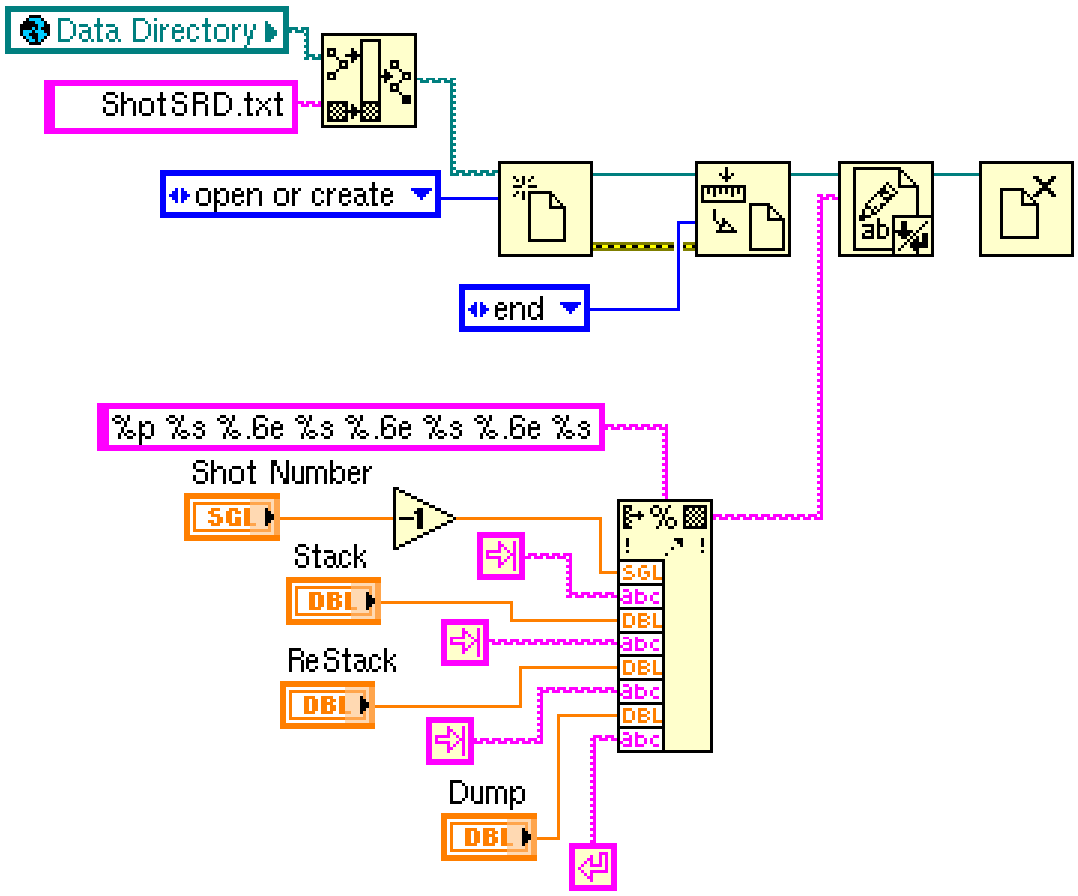

Figure A.9 WillSavePointsToFile.vi

Bibliography

[1] A. O. Benz, *Plasma Astrophysics: Kinetic Processes in Solar and Stellar Coronae*, 2nd ed. (Kluwer Academic Publishers, New York, NY, 2002).

[2] N. Sauthoff, "ITER Progress and Plans," presented at the 15th International Conference on Energing Nuclear Systems (San Francisco, CA, May 18, 2011).

[3] C. M. Surko, S. J. Gilbert, and R. G. Greaves, "Progress in creating low-energy positron plasmas and beams," AIP Conference Proceedings **498,** 3–12 (1999).

[4] W. Bertsche *et al.*, "A magnetic trap for antihydrogen confinement," Nuclear Instruments and Methods in Physics Research Section A: Accelerators, Spectrometers, Detectors and Associated Equipment **566,** 746 – 756 (2006).

[5] K. S. F. A. Collaboration, "The ATHENA antihydrogen experiment," AIP Conference Proceedings **498,** 40–47 (1999).

[6] A. G. Marshall, C. L. Hendrickson, and G. S. Jackson, "Fourier transform ion cyclotron resonance mass spectrometry: A primer," Mass Spectrometry Reviews **17,** 1–35 (1998).

[7] A. Peurrung, R. Kouzes, and S. Barlow, "The non-neutral plasma: an introduction to physics with relevance to cyclotron resonance mass spectrometry," International Journal of Mass Spectrometry and Ion Processes **157Ű158,** 39 – 83 (1996).

[8] T. Tamano and I. Katanuma, "Confinement properties of non-neutral and neutral plasmas in an axially symmetric system," AIP Conference Proceedings **606,** 556–561 (2002).

[9] E. G. Adelberger *et al.*, "Solar fusion cross sections," Rev. Mod. Phys. **70,** 1265–1291 (1998).

[10] M. Hutchinson, "Computational Analysis of the Relative Decay Constants for ^{7}Be, $^{7}Be^{+}$, AND $^{7}Be^{++}$,", Brigham Young University, Undergraduate thesis, 2009.

[11] I. B. Bernstein, "Waves in a Plasma in a Magnetic Field," Phys. Rev. **109,** 10–21 (1958).

[12] S. J. Buchsbaum and A. Hasegawa, "Longitudinal Plasma Oscillations near Electron Cyclotron Harmonics," Phys. Rev. **143,** 303–309 (1966).

[13] R. W. Gould and M. A. LaPointe, "Cyclotron resonance in a pure electron plasma column," Phys. Rev. Lett. **67,** 3685–3688 (1991).

[14] F. F. Chen, *Introduction to Plasma Physics and Controlled Fusion*, 2nd ed. (Springer, 223 Spring Street, New York, NY, 1984), Vol. 1.

[15] L. Turner, "Brillouin limit for non-neutral plasma in inhomogeneous magnetic fields," Physics of Fluids B: Plasma Physics **3,** 1355–1363 (1991).

[16] D. K. Olson, Master's thesis, Brigham Young University, 2007.

[17] C.-A. Huh, "Dependence of the decay rate of 7Be on chemical forms," Earth and Planetary Science Letters **171,** 325 – 328 (1999).

[18] X.-P. Huang, F. Anderegg, E. M. Hollmann, C. F. Driscoll, and T. M. O'Neil, "Steady-State Confinement of Non-neutral Plasmas by Rotating Electric Fields," Phys. Rev. Lett. **78,** 875–878 (1997).

[19] J. H. Malmberg and J. S. deGrassie, "Properties of Nonneutral Plasma," Phys. Rev. Lett. **35,** 577–580 (1975).

[20] R. F. Leininger, E. Segrè, and C. Wiegand, "Experiments on the Effect of Atomic Electrons on the Decay Constant of Be^7. II," Phys. Rev. **76,** 897–898 (1949).

[21] K. Giraud, "Simulation and Manufacture of a Quadrupole Mass Filter,", Brigham Young University Undergraduate thesis, 2008.

[22] C. Willams, "Electron Elimination As a Step Toward Long-Term Non-Neutral Ion Plasma Confinement,", Brigham Young University, Honors thesis, 2011.